CHEMISTRY OF MATERIALS

pubs.acs.org/cm

Article

$Sn_{4-\delta}B_{12}Se_{12}[Q_x]$, Q = Se, Te, a B_{12} Cluster Tunnel Framework Hosting Neutral Chalcogen Chains

Daniel G. Chica, Ioannis Spanopoulos, Shiqiang Hao, Chris Wolverton, and Mercouri G. Kanatzidis*

Cite This: *Chem. Mater.* 2021, 33, 1723−1730

Read Online

ACCESS | Metrics & More | Article Recommendations | Supporting Information

ABSTRACT: We report the open framework semiconductor, $Sn_4B_{12}Se_{12}$, synthesized using a Sn/Se flux method. The framework in this compound features the rare icosahedral $[B_{12}Se_{12}]^{14-}$ anion assembled into a 3D tunnel structure with open tunnels and is chemically stable over a wide pH range from concentrated nitric acid to 3 M NaOH aqueous solution. The rigid nature of this structure and high chemical stability allows chemical strategies for the removal of Se chains from the tunnels, giving an empty tunnel structure and subsequent insertion of tellurium chains as confirmed through single-crystal X-ray diffraction. The as-synthesized $Sn_4B_{12}Se_{12}[Se_{3.80}]$ contains selenium chains in the tunnels and crystallizes in the hexagonal space group $P6_322$ with $a = b = 13.5927(7)$ Å, $c = 9.8167(5)$ Å. After removal of Se and subsequent Te insertion, the space group remains the same with small changes in lattice parameters and occupancy of tin sites. The experimentally obtained optical band gap of the as-synthesized material is 1.66 eV and can be modulated by chemical modifications. DFT calculations of the empty framework show an indirect nature of the band gap calculated at 1.16 eV. The neutral framework of $Sn_4B_{12}Se_{12}$ is a new example of a microporous semiconductor with exceptional stability and electronic properties that stem from the presence of icosahedral boron clusters.

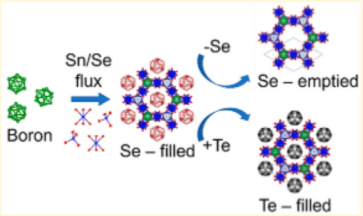

INTRODUCTION

A special property of the boron atom is the electron deficiency, which results in unique chemistry[1] yielding many interesting cluster species including many *closo*-borane anions, such as the dodecahedral cluster $B_{12}H_{12}^{2-}$,[2,3] which exhibits a particular chemical stability and does not react with air or water. These *closo*-borane clusters exhibit strong thermodynamic stability and high activation energy to reaction including oxidation and are often referred to as "aromatic"[4] because of the delocalization and resonance stabilization, resulting in a large energy gap between the highest occupied molecular orbital (HOMO) and lowest unoccupied molecular orbital (LUMO).

Compounds with boron−chalcogen bonds comprise the chalcoborate class, which features a variety of structural motifs typically with B^{3+} in either a trigonal or tetrahedral coordination. For example, binary boron sulfides crystallize in structures containing molecular to polymeric units such as porphyrin-like B_8S_{16}[5] or polymeric $(BS_2)_n$,[6] whereas ternary and quaternary boron chalcogenides feature anionic species with trigonal B atoms such as $(B(S/Se)_3)^{3-}$,[7] $(B_2S_5)^{2-}$,[8] and $(B_3S_6)^{3-}$,[9] and even corner-sharing BS_4 tetrahedra, as observed in the framework compounds $Li_9B_{19}S_{33}$ and $Li_{4-2x}Sr_{2+x}B_{10}S_{19}$ ($x = 0.27$).[10] A common characteristic of these chalcoborate phases is that they are very moisture sensitive and difficult to handle. The reason for this instability is the hard Lewis acid nature of B^{3+}, which generates intrinsic reactivity of the B−Q bond toward water and acids in a strongly exothermic reaction to produce very stable B−O bonds. Silica ampules typically used for most chalcogenide chemistry are inappropriate because boron chalcogenides will react with silicon dioxide to form silicon chalcogenides and boron oxides, resulting in silicon inclusion and rupturing of the ampule. Therefore, boron nitride, graphite, or amorphous carbon crucibles must be used. Because of these synthetic and practical challenges, boron chalcogenide chemistry has remained relatively underexplored.[11]

Because of the oxidizing nature of chalcogen toward boron, most compounds have B^{3+}, but there exist a few examples of framework compounds featuring partially oxidized B atoms in the form of *closo* B_{12} clusters. The $(A_3X)[MB_{12}(MQ_4)_3]$ (A = K, Cs; X = Cl, Br, I; M = Ga, In, Gd; Q = S, Se)[12,13] family of compounds consists of $[B_{12}Q_{12}]^{14-}$ anions that are linked together by M^{3+} cations to form an anionic framework with parallel tunnels. The negative charge is compensated by $[A_3X]^{2+}$, which fills the tunnels. There exists an analogue with a neutral framework, $CrSi_3B_{12}Se_{12}[B_2Se_3]_x$,[14] where Si^{4+} and Cr^{2+} are the linking cations while the tunnels are filled with B_2Se_3.

We describe here the open framework compound $Sn_4B_{12}Se_{12}$ synthesized from a Sn/Se flux using carefully selected synthetic techniques to circumvent the aforementioned challenges. This compound features 11 Å pores based on the distances between

Received: November 22, 2020
Revised: February 6, 2021
Published: February 25, 2021

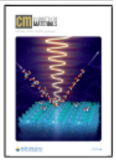

Table 1. Crystal Data and Structure Refinement for $Sn_{4-\delta}B_{12}Se_{12}[Q]$, Q = Se, Te, Compounds for Structure Models That Model Electron Density in the Pores[a]

empirical formula	$Sn_4B_{12}Se_{15.80}$	$Sn_{3.92}B_{12}Se_{12.61}$	$Sn_{3.88}B_{12}Se_{12}Te_{3.53}$
formula weight	1851.65	1591.23	1986.95
temperature	293 K	300 K	300 K
wavelength	0.71073 Å	0.71073 Å	1.54178 Å
crystal system	hexagonal	hexagonal	hexagonal
space group	$P6_322$	$P6_322$	$P6_322$
unit cell dimensions	a = 13.5927(7) Å, α = 90°	a = 13.6345(5) Å, α = 90°	a = 13.6603(6) Å, α = 90°
	b = 13.5927(7) Å, β = 90°	b = 13.6345(5) Å, β = 90°	b = 13.6603(6) Å, β = 90°
	c = 9.8167(5) Å, γ = 120°	c = 9.7695(4) Å, γ = 120°	c = 9.7630(5) Å, γ = 120°
volume	1570.8(2) Å^3	1572.8(1) Å^3	1577.7(2) Å^3
Z	2	2	2
density (calculated)	3.915 g/cm^3	3.360 g/cm^3	4.182 g/cm^3
absorption coefficient	21.443 mm^{-1}	17.667 mm^{-1}	65.155 mm^{-1}
F (000)	1594	1370	1690
crystal size (mm)	0.032 × 0.048 × 0.246	0.026 × 0.034 × 0.135	0.015 × 0.019 × 0.099
θ range for data collection	2.702−29.984°	1.725−29.975°	3.736−68.168°
index ranges	$-17 \le h \le 19$	$-19 \le h \le 19$	$-14 \le h \le 16$
	$-19 \le k \le 19$	$-18 \le k \le 16$	$-12 \le k \le 15$
	$-13 \le l \le 13$	$-13 \le l \le 13$	$-10 \le l \le 11$
reflections collected	16287	17436	8739
independent reflections	1546 [R_{int} = 0.0557]	1550 [R_{int} = 0.0454]	962 [R_{int} = 0.0355]
completeness to θ = 25.242°	99.8%	100%	99.8%
refinement method	full-matrix least-squares on F^2	full-matrix least-squares on F^2	full-matrix least-squares on F^2
data/restraints/parameters	1546/0/79	1550/0/61	962/0/95
goodness-of-fit	1.048	1.075	1.153
final R indices [$I > 2\sigma(I)$]	R_{obs} = 0.0166, wR_{obs} = 0.0372	R_{obs} = 0.0141, wR_{obs} = 0.0311	R_{obs} = 0.0215, wR_{obs} = 0.0505
R indices [all data]	R_{all} = 0.0190, wR_{all} = 0.0378	R_{all} = 0.0150, wR_{all} = 0.0314	R_{all} = 0.0230, wR_{all} = 0.0508
extinction coefficient	N/A	N/A	N/A
largest diff. peak and hole	0.670 and −0.586 e·Å^{-3}	0.345 and −0.577 e·Å^{-3}	0.506 and −0.434 e·Å^{-3}

[a] $R = \sum||F_o| - |F_c||/\sum|F_o|$, $wR = \{\sum[w(|F_o|^2 - |F_c|^2)^2]/\sum[w(|F_o|^4)]\}^{1/2}$. $Sn_4B_{12}Se_{15.80}$: $w = 1/[\sigma^2(F_o^2) + (0.0140P)^2 + 0.3009P]$. $Sn_{3.92}B_{12}Se_{12.6}$: $w = 1/[\sigma^2(F_o^2) + 0.4631P]$. $Sn_{3.88}B_{12}Se_{12}Te_{3.53}$: $w = 1/[\sigma^2(F_o^2) + (0.0158P)^2 + 4.5572P]$. $P = (F_o^2 + 2F_c^2)/3$.

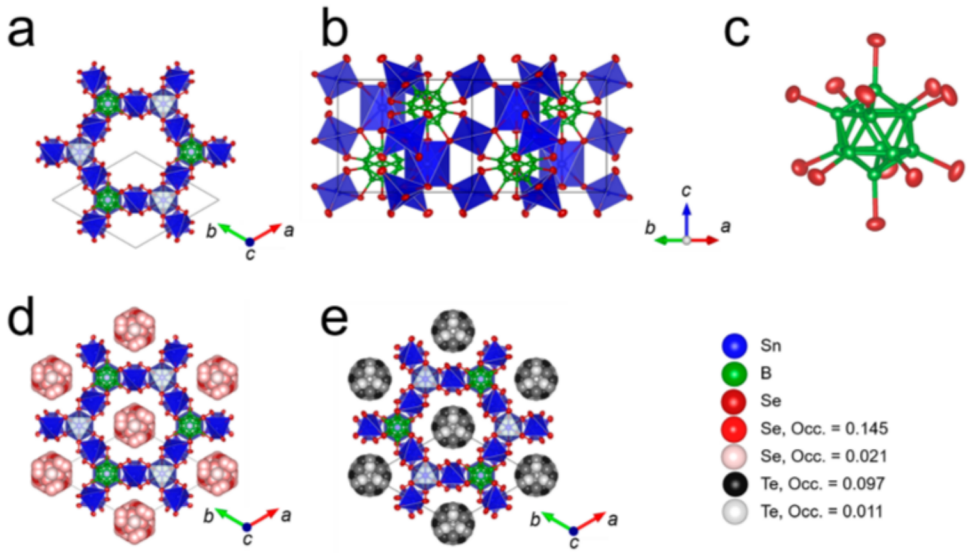

Figure 1. Crystal structure of the $Sn_4B_{12}Se_{12}$ framework oriented down the (a) ⟨001⟩ (with empty tunnels running in this direction) and (b) ⟨110⟩ of an extended cell. (c) Isolated $[B_{12}Se_{12}]^{14-}$ *closo*-borane cluster showing icosahedral symmetry. Crystal structure of (d) $Sn_4B_{12}Se_{12}[Se_{3.80}]$ and (e) $Sn_{3.88}B_{12}Se_{12}[Te_{3.53}]$ down the ⟨001⟩ (with filled tunnels). The color of the highest and lowest occupancy for the chalcogen in the pore can be seen in the legend. The brightness of the color corresponds to the occupancy.

selenium atoms on the wall of the pores. $Sn_4B_{12}Se_{12}[Se_{3.80}]$ exhibits extreme pH stability from concentrated HCl/nitric acid to 3 M NaOH, in stark contrast to the chemical sensitivity of most boron chalcogenides. This compound belongs to the broader class of microporous semiconductors,[15−19] has an optical band gap of 1.66 eV, and transitions into a collapsed state from 650 to 825 °C. Heating this material in molten selenium at 500 °C followed by heat treatment in a

https://dx.doi.org/10.1021/acs.chemmater.0c04503
Chem. Mater. 2021, 33, 1723−1730

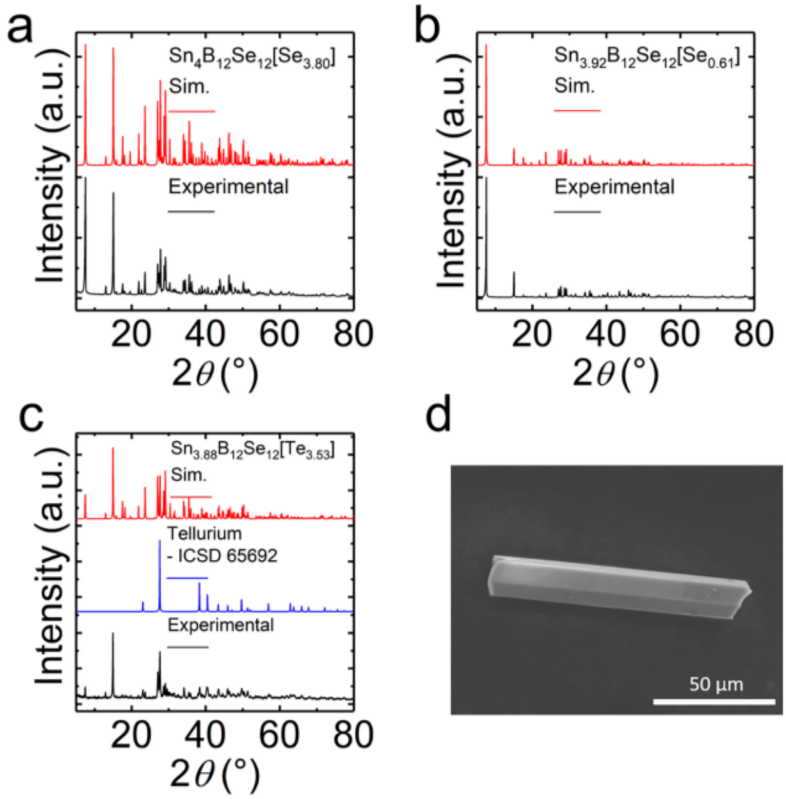

Figure 2. Experimental and simulated PXRD pattern for (a) $Sn_4B_{12}Se_{12}[Se_{3.80}]$, (b) $Sn_{3.92}B_{12}Se_{12}[Se_{0.61}]$, and (c) $Sn_{3.88}B_{12}Se_{12}[Te_{3.53}]$. Tellurium was a secondary phase in the $Sn_{3.88}B_{12}Se_{12}[Te_{3.53}]$ reaction. (d) SEM image of isolated $Sn_{3.88}B_{12}Se_{12}[Te_{3.53}]$ crystal.

temperature gradient (T_{hot} = 600−500 °C, T_{cold} = ∼25 °C) removed a significant portion of the species inside the pores without affecting the framework, as confirmed by single-crystal diffraction analysis. Tellurium was then exchanged with selenium from the pores of the $Sn_4B_{12}Se_{12}$ framework by reacting the as-synthesized material with an excess of tellurium at 550 °C. This example of successful postsynthesis manipulation suggests that the pores in the structure are accessible for performing insertion/deinsertion chemistry using various guest molecular species.

■ RESULTS AND DISCUSSION

Crystal Structure of As-Synthesized $Sn_4B_{12}Se_{12}[Se_{3.80}]$. $Sn_4B_{12}Se_{12}[Se_{3.80}]$ was synthesized from a Sn/Se flux and it crystallizes in the chiral hexagonal space group $P6_322$ with lattice parameters $a = b = 13.5927(7)$ Å and $c = 9.8167(5)$ Å (details of the crystallographic refinement are given in Table 1). The three-dimensional framework is comprised of $(B_{12}Se_{12})^{14-}$ anionic *closo*-borane clusters (see Figure 1c) that are connected along the *c* axis by octahedral Sn^{2+} centers, forming infinite parallel $[SnB_{12}Se_{12}]^{12-}$ columns. These then connect in the *a*/*b* directions to three other columns via tetrahedral Sn^{4+} cations, forming B−Se−Sn^{4+} bonds, which yields the honeycomb tunnel structure seen in Figure 1a. The structure can be visualized through another perspective showing the arrangement of the tin selenide octahedra bridging the $(B_{12}Se_{12})^{14-}$ clusters along *c* as well as the tin selenide tetrahedra bridging the same clusters along *a*, *b* (see Figure 1b).

The Wade-Mingos rules state that for polyhedral *closo*-boranes with general formula $B_nH_n^{2-}$, the skeletal electrons needed are $2n + 2$.[1] This same electron counting rule for the skeletal electrons can be applied to the $(B_{12}Se_{12})^{14-}$ anionic cluster as the core B_{12} cluster is the same. With n = 12, 26 electrons are needed for skeletal bonding, which can be supplied by the 36 valence electrons of boron. This leaves 10 electrons for bonding with selenium. Combined with the 14 electrons supplied by the tin atoms ($3Sn^{4+}$,$1Sn^{2+}$), the selenium atoms would have a full octet. Thus, the framework would be electrically neutral.

The bond lengths and coordination environment give evidence to the valence of the tin cations. The Sn−Se bond lengths (3.0299(3) Å) for the octahedral tin are consistent with other Sn^{2+} selenides.[20] For the tetrahedral Sn−Se bonds, the bond lengths (2.5080(4)−2.5564(5) Å) were close to the literature values for Sn^{4+} selenides in tetrahedral sites.[21,22] The distances between the selenide anions from opposite walls of the pores range from 10.854(2) to 10.984(2) Å.

After the atoms of the framework were successfully located during the structure solution, a significant amount of additional diffuse electron density was present in the tunnels, suggesting they were occupied. Because the electron density was delocalized throughout the 11 Å wide tunnels, suggesting positional disorder, the precise structure of the species in the pores could not be definitively determined through diffraction. EDS analysis indicates the species in the pores is Se and the structure is therefore highly disordered Se chains based on a similar phenomenon of chalcogen chains inserted in the tunnel structures of $Ta_4P_4S_{29}$[23] and $TaPS_6Se$.[24] The chemical formula determined from EDS was $Sn_4B_{12}Se_{16.8}$, normalizing to tin and assuming a Sn/B ratio of 4:12 based on the crystal structure from SCXRD. The B ratio relative to tin or selenium could not

https://dx.doi.org/10.1021/acs.chemmater.0c04503
Chem. Mater. 2021, 33, 1723−1730

be determined through EDS because of the high overvoltage of the accelerating voltage. The chemical formula derived from semiquantative EDS analysis was slightly Se-rich compared to the formula determined from single-crystal structure, though within the error of the technique. The SEM image shown in Figure S4a (Supporting Information) demonstrates the rodlike morphology of the as-synthesized crystals.

Thus, we modeled the electron density using Se with isotropic thermal parameters to improve the refinement. Though the species in the pores was diffuse, the electron density exhibited a trihelix structure (Figure 1d, Figure S1). The isotropic thermal parameters of the Se atoms in the tunnels were constrained to be the same while the occupancy was freely refined. The thermal parameters of the selenium atoms in the pores were about an order of magnitude larger than the Se atoms of the framework, highlighting the positional disorder in the pores. In Table S1a, the R values were much lower for the model that accounts for the electron density in the pores compared to the values of the empty tunnel structure. The structure modeling the selenium in the pores can be seen in Figure 1d, showing selenium filling the entirety of the pore.

Formation of $Sn_4B_{12}Se_{12}[Se_{3.80}]$ under Various Synthetic Conditions. Initially, in our synthesis experiments we targeted phases containing boron in the +3 oxidation state but added a significant portion of a metal chalcogenide in the composition to impart better chemical stability in the resulting structure. Therefore, the nominal stoichiometry of $Sn_2BSe_{3.5}$ was selected. This reaction yielded SnSe and $SnSe_2$ as the major products with a small amount of $Sn_4B_{12}Se_{12}[Se_{3.80}]$ (Figure S5a,b). Small black rodlike crystals were mechanically separated for single-crystal X-ray diffraction analysis, yielding the structure of $Sn_4B_{12}Se_{12}[Se_{3.80}]$ described above. Then reactions with a stoichiometric ratio of the elements of the framework ($Sn_4B_{12}Se_{12}$) at 800 °C were attempted to produce phase-pure material of the empty $Sn_4B_{12}Se_{12}$ framework. This reaction, however, did not yield phase-pure products as seen in the PXRD (Figure S5c,d). Therefore, alternative synthesis routes were developed involving Sn/Se and B/Se reactive fluxes. $Sn_4B_{12}Se_{12}[Se_{3.80}]$ was synthesized using a Sn/Se flux at 885 °C, corresponding to the charge composition of "$SnBSe_{2.5}$". After heating, we observed that the $Sn_4B_{12}Se_{12}[Se_{3.80}]$ product was intermixed with various tin and boron selenides. The high chemical stability of $Sn_4B_{12}Se_{12}[Se_{3.80}]$ allowed the removal of these byproducts with a sequence of washings with concentrated nitric acid, aqueous NaOH, deionized water, and acetone. The rodlike morphology of the final product, which remarkably was not affected by concentrated nitric acid, aqueous NaOH, can be seen in Figure S4a. The phase purity was confirmed through PXRD (Figure 2a). When the Sn/Se flux reaction was subjected to a heating profile up to 1000 °C, an unknown phase with very broad diffraction peaks (Figure S5e) was observed, limiting the highest synthesis temperature for the flux reaction to ∼885 °C. In addition to the above procedures, the $Sn_4B_{12}Se_{12}[Se_{3.80}]$ compound can also be synthesized via a B/Se flux with a charge composition of $Sn_2B_{12}Se_{12}$. After removal of the boron selenide flux with water, the product was phase-pure, as confirmed with PXRD, though the crystallite size was smaller (<100 μm), compared to the material synthesized from the Sn/Se flux. Thus, the Sn/Se was the preferred method of synthesis.

Removal of Guest Species from the Tunnels. Examination of the single-crystal structure of as-synthesized $Sn_4B_{12}Se_{12}[Se_{3.80}]$ suggests that the pores of the charge-neutral 3D framework, which are filled with disordered species, could be cleared. This scenario mirrors the crystallographic disorder of solvent observed in MOFs, which can be removed and leave the framework intact.[25] Because the material is stable in alkaline solutions, it was soaked in 3 M NaOH for several days to attempt the removal of the species inside the pores. This route was not successful, as evidenced by the diffraction pattern of the material after soaking, which does not match the intensities of the simulated powder pattern of the empty structure seen in Figure S5f. Notably, the (100) Bragg reflection was a similar intensity to the (200) for the experimental pattern while the simulated empty structure exhibits much greater intensity for the (100) compared to that for the (200) peak. Because these intensities can be calculated for the empty as well as filled frameworks, their intensity ratio can be used to gauge the degree of pore filling.

Attempts to empty out the pores of the framework by heating the material to 600 °C to slowly evaporate away the selenium were partly successful because the framework was mostly emptied, as confirmed by PXRD (Figure S10a). The material that condensed close to the cold end ($T \sim 25$ °C) was confirmed to be selenium using PXRD (see Figure S10b), corroborating the pore species in the single-crystal model. The residue left in the pores resulted in the blockage of pores, precluding interaction with the atmosphere in contrast with the properly activated material discussed below (see Figure S10c,d). We speculated that the reason for this may be the presence of small amounts of Sn and/or B selenium bonded species in the tunnels that were less volatile. Even though the electron density inside the pores was modeled with selenium, there was the possibility that some tin or boron may have incorporated in the pores. We thus modified the procedure to involve treatment with excess selenium flux meant to equilibrate the pore contents so that these species can come out into the flux and be replaced by selenium. Thus, a more extreme route was attempted with the reaction of the material with an excess of selenium at 500 °C because the pore species would be very soluble under these conditions and the excess selenium could ensure the species inside the pore was entirely selenium. A heat treatment could then remove the loosely bound selenium from the tunnels by evaporation, leaving behind the nearly empty framework. The chemical stability and rigidity of the $Sn_4B_{12}Se_{12}$ framework would allow this material to survive this harsh chemical treatment and formation of a vacuum.

Since this process is a topotactic single-crystal to single-crystal transformation, after the selenium flux soak and heat treatment, a single-crystal crystallographic analysis was performed to observe the effect of these treatments on the structure of the as-synthesized $Sn_4B_{12}Se_{12}[Se_{3.80}]$. The crystal structure and details of the refinement of $Sn_{3.92}B_{12}Se_{12}[Se_{0.61}]$ are shown in Figure S2 and Table 1, respectively. While the space group remained the same as the as-synthesized compound ($P6_322$), there were notable changes to the structure. The amount of selenium per framework formula unit was reduced from 3.80 to 0.61. While the electron density of the filled structure had a spiral form, the electron density in the pores of the empty structure was uniform, as seen in Figure S2a,b. The a,b lattice parameters expanded ($a = b =$ 13.6345(5) Å) while the c (9.7695(4) Å) contracted. Overall,

https://dx.doi.org/10.1021/acs.chemmater.0c04503
Chem. Mater. 2021, 33, 1723−1730

the volume of the unit cell increased slightly from 1570.8(2) to 1572.8(1) Å^3, suggesting that the lack of guest−host interactions reduced the strain and enabled framework relaxation. The distances between selenide atoms on opposite sides of the tunnel wall ranged from 10.9141(3) to 11.0461(5) Å, a small increase from the as-synthesized structure. For the Sn^{2+} on the octahedral site, the occupancy and Sn−Se bond length decreased to 0.926(2) and 3.0128(3) Å, respectively. These changes suggested that some of the tin from this site was leeched into the Se flux and a fraction of the remaining tin was oxidized to Sn^{4+} to maintain charge balance. Both of these can account for the slight contraction along *c*. The occupancy on the tetrahedral tin site remains unchanged. The experimental PXRD pattern matches well with the simulated powder pattern (see Figure 2b). The chemical formula from the single-crystal structure agreed with the formula attained from semiquatitative EDS analysis of $Sn_{3.92}B_{12}Se_{11.92}$ (tin amount normalized to the amount determined from SCXRD). The chemical formula obtained through EDS was slightly selenium-deficient when compared to the formula from the single-crystal structure but illustrates the drastic reduction of selenium in the compound when the Se flux and heat treatment were applied. Sodium made up 3.6% of the atomic species of the emptied $Sn_{3.92}B_{12}Se_{12}[Se_{0.61}]$ according to EDS analysis, indicating residue from cleaning with aqueous NaOH. The sodium could potentially be located on the surface of the crystallites, the tunnels, or the octahedral vacancies left by the Sn^{2+}. The rodlike morphology of the emptied framework was maintained with a similar size distribution after the Se and heat treatment (Figure S4b), consistent with the topotactic nature of the phase transformation.

The response of $Sn_{3.92}B_{12}Se_{12}[Se_{0.61}]$ to air was monitored using PXRD in air as a function of time (Figure S9a−c). Over several hours, the intensity and position of several peaks were modulated in air, most notably the decrease in intensity of the (100) reflection, which signifies the backfilling of the tunnel with gas species from the atmosphere. This effect was not observed for material activated only by heat treatment, emphasizing the need for the molten Se treatment to properly activate the material (see Figure S10c,d).

Formation of $Sn_{3.88}B_{12}Se_{12}[Te_{3.53}]$ by Refilling the Tunnels through Tellurium Exchange. Given the success of the above procedure using the excess selenium flux, we hypothesized that a similar procedure using tellurium could replace the contents of the pores with mostly tellurium in a typical topotactic exchange reaction. Tellurium was exchanged with the selenium in $Sn_4B_{12}Se_{12}[Se_{3.80}]$ by annealing as-synthesized $Sn_4B_{12}Se_{12}[Se_{3.80}]$ with an excess of tellurium at 550 °C. Most of the excess tellurium aggregated together so it could be mechanically removed. A black, rodlike crystal was chosen for single-crystal diffraction measurements to identify changes to the structure with chemical treatment. The structure and refinement details for $Sn_{3.88}B_{12}Se_{12}[Te_{3.53}]$ are shown in Figure 1e and Table 1, respectively. The space group for this compound was the same as both $Sn_4B_{12}Se_{12}[Se_{3.80}]$ and $Sn_{3.92}B_{12}Se_{12}[Se_{0.61}]$. The *a*/*b* lattice parameter and volume were 13.6603(6) Å and 1577.7(2) Å^3, respectively, the largest compared to those of the other compounds, suggesting an overall expansion of the tunnel and framework from the inclusion of this larger species compared to that of selenium. The tellurium flux had a similar effect on the octahedral tin occupancy as the selenium flux as the occupancy was reduced from 1 to 0.874(6). This reduction in occupancy had a similar effect on decreasing the *c* lattice parameter relative to the as-synthesized material described above where partial oxidation of the Sn^{2+} to Sn^{4+} and vacancies will cause the framework to contract along the *c*-axis. The electron density inside the pores was also diffuse and therefore was modeled with tellurium using the same model as the previous structure solution. The refinement was greatly improved when the tellurium in the pore was modeled (see Table S1c) with a tellurium occupancy of 3.53 per formula unit.

The PXRD of $Sn_{3.88}B_{12}Se_{12}[Te_{3.53}]$ samples shows a two-phase mixture of the Te-filled phase and tellurium (Figure 2c). The (100) Bragg reflection was much less intense than the (200) reflection, in accordance with the $Sn_{4-\delta}B_{12}Se_{12}$ framework being filled with a high *Z* element. This reduction was more pronounced compared to the pattern derived from the single-crystal structure, meaning the bulk powder possibly contains more tellurium in the pores than determined from the selected single crystal. The average formula derived from EDS analysis was $Sn_{3.88}B_{12}Se_{12.44}Te_{3.33}$, which agreed with the formula derived from single-crystal diffraction. Similar to the case of the emptied framework, the topotactic insertion of the tellurium chains from the tellurium flux treatment does not change the rodlike morphology shown in a SEM image of a Te-treated crystal shown in Figure 2d.

Thermal Properties and Temperature-Dependent Structural Changes of $Sn_{3.92}B_{12}Se_{12}[Se_{0.61}]$. The thermal properties of $Sn_{3.92}B_{12}Se_{12}[Se_{0.61}]$ were investigated with differential thermal analysis up to 1000 °C. The heat flow versus temperature plot seen in Figure S6a shows a small endothermic feature at 905 °C, which was not present on the second heating cycle. Thermal events were not detected on cooling. The post-DTA PXRD (Figure S6b) shows the compound became amorphous from heating to 1000 °C at a rate of 10 K/min. The material remained a loose powder, indicating the material did not sinter or melt.

Because the temperature of the transition event was not very clear using DTA, variable temperature PXRD was measured on $Sn_{3.92}B_{12}Se_{12}[Se_{0.61}]$ to better pinpoint the onset temperature. The diffraction patterns of $Sn_{3.92}B_{12}Se_{12}[Se_{0.61}]$ at temperatures from ambient temperature up to 1000 °C are shown in Figure S7a. The compound exhibited thermal expansion up to 650 °C, and from 400 to 650 °C, the (100) reflection increased in intensity, signifying a lowering of the occupancy of species in the pores. From 650 to 825 °C, the (100) peak decreased to effectively zero intensity while other peaks shifted to higher 2θ angles. This effect can be attributed to the collapse of the framework structure. In contrast to the results of the DTA experiment, a crystalline material remained after the VTPXRD experiment, which we attribute to the difference in heating rates (DTA heating rate = 10 K/min vs VTPXRD average heating rate = 1.25 K/min). The slower heating rate allows the empty structure to slowly relax into a collapsed crystalline state. The thermal event at 905 °C observed in the DTA experiment corresponds to a slight structural change of the collapsed framework compound deduced by the shifting of reflections in the VT diffractograms at 900 °C. The material was heated ex situ to 500 °C at a rate of 1.3 K/min, then heated to 1000 °C at a rate of 0.35 K/min, and cooled to ambient temperature in 12 h. The PXRD pattern (Figure S8) shows Bragg reflections of the collapsed material in addition to an amorphous background, corroborating the results of the VTPXRD measurement.

https://dx.doi.org/10.1021/acs.chemmater.0c04503
Chem. Mater. 2021, 33, 1723−1730

Optical Band Gap and Electronic Band Structure. The optical band gap of all the samples was derived from UV−vis diffuse reflectance measurements seen in Figure 3. The band

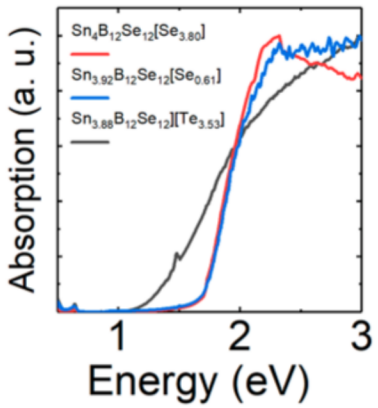

Figure 3. Optical absorbance spectra of $Sn_4B_{12}Se_{12}[Se_{3.80}]$, $Sn_{3.92}B_{12}Se_{12}[Se_{0.61}]$, and $Sn_{3.88}B_{12}Se_{12}[Te_{3.53}]$.

gaps of $Sn_4B_{12}Se_{12}[Se_{3.80}]$ and $Sn_{3.92}B_{12}Se_{12}[Se_{0.61}]$ were 1.66 and 1.69 eV, respectively. The slight blue shift in the band gap of the empty framework was due to a small narrowing of the electronic band widths of the valence band as this band was partially comprised of Sn 5p states from the octahedral tin. The presence of mass inside the pores involves significant van der Waals contacts between the guest species and the host framework, which typically has the effect of slightly broadening electronic bands via orbital overlap. By comparison, the related $[K_3I]In_4B_{12}Se_{12}$ compound has a slightly higher band gap of 1.97 eV.[13] The Te-filled $Sn_{3.88}B_{12}Se_{12}[Te_{3.53}]$ demonstrated a red shift in the band gap to 1.32 eV, which is attributed to the band gap of isolated 1D chains of Te and masks the band gap of the framework.

The electronic band structure was calculated for the empty framework only because the uncertainty and disorder in the chalcogen chain atoms inside the pores did not allow for a proper model to be used for the filled case. The calculations shown in Figure 4a reveal that the $Sn_4B_{12}Se_{12}$ framework as an indirect semiconductor with a band gap of 1.16 eV with the valence band maxima at some point along the Γ−A (0, 0, 0 → 0, 0, $^1/_2$) and the conduction band minima at the *K* ($^1/_3$, $^1/_3$, 0) point. This calculation underestimates the band gap when compared to the measured optical band gap, as is common for DFT calculations. The conduction band minimum (CBM) is comprised of Se 4p, Sn_{oct} 5p, and Sn_{tet} 5s orbitals while the valence band maximum (VBM) is made up of Se 4p and Sn_{oct} 5s orbitals (see Figure 4b). While the B 2p orbitals are not involved with the bands that form either the CBM and VBM, they hybridize with Se 4p and Sn 5p states to form bands below and above the VBM and CBM, respectively. This large gap between these bonding and antibonding bands are reminiscent of the large HOMO−LUMO gap of the molecular $B_{12}H_{12}$ *closo*-cluster. Thus, we attribute the chemical stability of the framework to this large gap. The conduction band is comprised of relatively flat bands, implying low electron mobility. The valence band has certain directions that are relatively disperse, such as the H to K ($^1/_3$, $^1/_3$, $^1/_2$ → $^1/_3$, $^1/_3$, 0) and L to M ($^1/_2$, 0, $^1/_2$ → $^1/_2$, 0, 0) direction. However, other directions are extremely flat such as the A to L (0, 0, $^1/_2$ → $^1/_2$, 0, $^1/_2$) and A to H (0, 0, $^1/_2$ → $^1/_3$, $^1/_3$, $^1/_2$) directions. The indirect nature of the band structure manifests experimentally from the shallow slope of the band edge from diffuse reflectance measurements.

■ CONCLUSIONS

The open B_{12} borane cluster-based framework compound $Sn_4B_{12}Se_{12}$ formed from reaction in a Sn/Se flux. This material is extremely stable under severe chemical treatments because of the chemical stability of the *closo*-B_{12} clusters, in contrast to the chemically sensitive nature of most other compounds in the chalcoborate class. The $Sn_4B_{12}Se_{12}$ framework is electrically neutral and has parallel tunnels that are large enough to accommodate neutral chains of neutral chalcogen atoms. The weakly bound nature of the selenium in the tunnel pores allows their topotactic removal, leaving an empty tunnel framework that can then be filled with other species such as tellurium chains. The band gap of these materials ranged from 1.32 to 1.69 eV, which are lower compared to other porous materials such as zeolites and metal−organic frameworks, the majority being insulators. Coupled with its high thermal stability, the porous $Sn_4B_{12}Se_{12}$ compound and its derivatives could be used for new types of insertion/deinsertion reaction chemistry to introduce novel species inside the tunnels. This new accessible framework will be of interest in gas sensing and separation, heterogeneous catalysis, and ion sequestration.

■ EXPERIMENTAL SECTION

Optimized Flux Synthesis of $Sn_4B_{12}Se_{12}[Se_{3.80}]$. The tin, boron, and selenium reagents were loaded into a 12.7 mm graphite crucible with a lid (i.d. 11 mm). The Sn/B/Se ratio used was 1:1:2.5, corresponding to 0.3307 g (30.59 mmol) of B, 3.6312 g (30.59 mmol) of Sn, and 6.0382 g (76.47 mmol) of Se. The charged crucible was placed into a fused silica tube (o.d. 15 mm, i.d. 13 mm) and

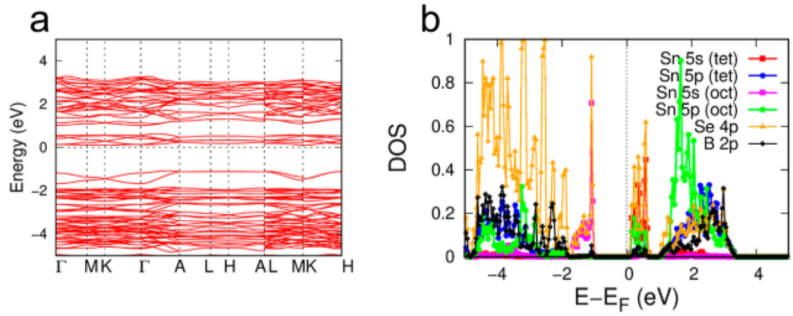

Figure 4. (a) Calculated electronic band structure and (b) density of states plot of the $Sn_4B_{12}Se_{12}$ framework (no species in the pores).The high-symmetry points have coordinates as follows: Γ (0, 0, 0), M ($^1/_2$, 0, 0), K ($^1/_3$, $^1/_3$, 0), A (0, 0, $^1/_2$), L ($^1/_2$, 0, $^1/_2$), and H ($^1/_3$, $^1/_3$, $^1/_2$).

https://dx.doi.org/10.1021/acs.chemmater.0c04503
Chem. Mater. 2021, 33, 1723−1730

flame-sealed under ~3 × 10^{-3} mbar of pressure. This reaction vessel was placed in a tilted, computer-controlled tube furnace and set to the following heating profile: Heat to 375 °C in 6 h, hold for 12 h, heat to 885 °C in 12 h, hold for 6 h, cool to 500 °C in 12 h, turn off furnace, and cool to ambient temperature. The following steps were performed in a well-ventilated fume hood because noxious gas of H_2Se and NO_2 were evolved in the following steps. The black ingot containing the flux and product were removed from the graphite crucible and then broken up in a mortar and pestle to approximately 1 mm sized chunks. The material was put into a 50 mL centrifuge tube with 20 mL of concentrated nitric acid. The addition of nitric acid oxidizes the SnSe/$SnSe_2$ flux material and produces a gray precipitate while leaving the $Sn_4B_{12}Se_{12}[Se_{3.80}]$ intact. After 2 h, the mixture was centrifuged at 4000 rpm and the supernatant was pipeted away and discarded. A 20 mL aliquot of deionized water was added, followed by NaOH pellets. The pellets were added at a rate of 1 s^{-1} because the reaction of the pellets with the precipitate is highly exothermic and would cause the mixture to overflow. The pellets were added until the mixture stopped bubbling, which was approximately 3 g of NaOH. The mixture was centrifuged at 4000 rpm and the deep red supernatant was pipeted away and discarded. Then 20 mL of 3 M NaOH aqueous solution was added to the centrifuge tube and allowed to dissolve residual impurities for about 10 min followed by centrifugation and disposal of the supernatant. This process was repeated until the supernatant was clear. The previous step was repeated twice again for deionized water and then once with acetone.

Removal of Se from $Sn_4B_{12}Se_{12}[Se_{3.80}]$ to Form $Sn_{3.92}B_{12}Se_{12}[Se_{0.61}]$. In a typical reaction, 1.00 g (0.540 mmol) of as-synthesized $Sn_4B_{12}Se_{12}[Se_{3.80}]$ and 4.00 g (50.7 mmol) of selenium shot were loaded into a fused silica tube (o.d. 10 mm, i.d. 9 mm). The tube was flame-sealed under ~3 × 10^{-3} mbar of pressure, put into a tilted tube furnace, and subjected to the following heating profile: heat to 500 °C in 12 h, hold for 168 h, and cool to ambient temperature in 12 h. The tube was opened, and the material was transferred into a fused silica tube (o.d. 12.7 mm, i.d. 10.5 mm) and then flame-sealed under ~3 × 10^{-3} mbar of pressure. The length of the tube after flame sealing was ~25 cm. The tube was placed in a horizontal tube furnace with the side of the tube with the material at the center of the furnace and the other side of the tube sticking out of the furnace about 4 cm. The side of the tube with the product was subjected to the following heating profile: heat to 500 °C in 12 h, hold for 168 h, and cool to ambient temperature in 12 h. The tube was then opened, and the PXRD pattern was collected. After scanning, the product was resealed in a fused silica tube (o.d. 12.7 mm, i.d. 10.5 mm) to a length of ~25 cm, placed in the furnace as described above, and subjected to the following heating profile: heat to 600 °C in 12 h, hold for 96 h, and cool to ambient temperature in 12 h.

Tellurium Insertion into $Sn_4B_{12}Se_{12}[Se_{3.80}]$ Framework to Form $Sn_{3.88}B_{12}Se_{12}[Te_{3.53}]$. In a typical reaction, 65 mg (0.035 mmol) of as-synthesized $Sn_4B_{12}Se_{12}[Se_{3.80}]$ and 2.00 g (15.7 mmol) of Te were loaded into a fused silica tube (o.d. 10 mm, i.d. 9 mm) and then flame-sealed under ~3 × 10^{-3} mbar of pressure. The tube was subjected to the following heating profile: Heat to 550 °C in 12 h, anneal for 96 h, and cool to ambient temperature in 12 h. Most of the tellurium aggregated into a single lump, which was mechanically removed from the loose powder of the product.

■ ASSOCIATED CONTENT

Supporting Information

The Supporting Information is available free of charge at https://pubs.acs.org/doi/10.1021/acs.chemmater.0c04503.

Supplemental experimental section, crystal structures, PXRD, VTPXRD, DTA, Raman spectra, and crystallographic details (PDF)

X-ray crystallographic data for $Sn_{3.92}B_{12}Se_{12}[Se_{0.61}]$; Formula: $Sn_4B_{12}Se_{12.61}$ (CIF)

X-ray crystallographic for data $Sn_{3.88}B_{12}Se_{12}[Te_{3.53}]$; Formula: $Sn_{3.88}B_{12}Se_{12}Te_{3.53}$ (CIF)

X-ray crystallographic data for $Sn_4B_{12}Se_{12}[Se_{3.80}]$; Formula: $Sn_4B_{12}Se_{15.80}$ (CIF)

■ AUTHOR INFORMATION

Corresponding Author

Mercouri G. Kanatzidis − *Department of Chemistry, Northwestern University, Evanston, Illinois 60208, United States;* orcid.org/0000-0003-2037-4168; Email: m-kanatzidis@northwestern.edu

Authors

Daniel G. Chica − *Department of Chemistry, Northwestern University, Evanston, Illinois 60208, United States;* orcid.org/0000-0001-8616-9365

Ioannis Spanopoulos − *Department of Chemistry, Northwestern University, Evanston, Illinois 60208, United States;* orcid.org/0000-0003-0861-1407

Shiqiang Hao − *Department of Materials Science and Engineering, Northwestern University, Evanston, Illinois 60208, United States;* orcid.org/0000-0002-7985-4468

Chris Wolverton − *Department of Materials Science and Engineering, Northwestern University, Evanston, Illinois 60208, United States;* orcid.org/0000-0003-2248-474X

Complete contact information is available at: https://pubs.acs.org/10.1021/acs.chemmater.0c04503

Notes

The authors declare no competing financial interest.

■ ACKNOWLEDGMENTS

This work was supported by the National Science Foundation through Grant DMR-2003476. This work made use of the IMSERC X-RAY facility at Northwestern University, which has received support from the Soft and Hybrid Nanotechnology Experimental (SHyNE) Resource (NSF ECCS-1542205), and Northwestern University. This work made use of the EPIC facility of Northwestern University's NUANCE Center, which has received support from the SHyNE Resource (NSF ECCS-2025633), Northwestern's MRSEC program (NSF DMR-1720139), the Keck foundation, and the State of Illinois through IIN.

■ REFERENCES

(1) King, R. B. Three-Dimensional Aromaticity in Polyhedral Boranes and Related Molecules. *Chem. Rev.* **2001**, *101* (5), 1119−1152.

(2) Udovic, T. J.; Matsuo, M.; Unemoto, A.; Verdal, N.; Stavila, V.; Skripov, A. V.; Rush, J. J.; Takamura, H.; Orimo, S. I. Sodium Superionic Conduction in $Na_2B_{12}H_{12}$. *Chem. Commun.* **2014**, *50* (28), 3750−3752.

(3) Pitt, M. P.; Paskevicius, M.; Brown, D. H.; Sheppard, D. A.; Buckley, C. E. Thermal Stability of $Li_2B_{12}H_{12}$ and Its Role in the Decomposition of $LiBH_4$. *J. Am. Chem. Soc.* **2013**, *135* (18), 6930−6941.

(4) Poater, J.; Solà, M.; Viñas, C.; Teixidor, F. π Aromaticity and Three-Dimensional Aromaticity: Two Sides of the Same Coin. *Angew. Chem., Int. Ed.* **2014**, *53* (45), 12191−12195.

(5) Krebs, B.; Hurter, H. U. B_8S_{16} - An "Inorganic Porphine. *Angew. Chem., Int. Ed. Engl.* **1980**, *19* (6), 481−482.

(6) Krebs, B. Thio- and Seleno-Compounds of Main Group Elements—Novel Inorganic Oligomers and Polymers. *Angew. Chem., Int. Ed. Engl.* **1983**, *22* (2), 113−134.

(7) Krebs, B.; Hamann, W. Ortho-Thioborates and Ortho-Selenoborates: Synthesis, Structure and Properties of Tl_3BS_3 and Tl_3BSe_3. *J. Less-Common Met.* **1988**, *137* (1−2), 143−154.
(8) Jansen, C.; Küper, J.; Krebs, B. $Na_2B_2S_5$ and $Li_2B_2S_5$: Two Novel Perthioborates with Planar 1,2,4-Trithia-3,5-Diborolane Rings. *Z. Anorg. Allg. Chem.* **1995**, *621* (8), 1322−1329.
(9) Püttmann, C.; Diercks, H.; Krebs, B. Synthesis, Crystal Structures and Properties of $M_3B_3S_6$ (M = Na, K, Rb) and $LiSrB_3S_6$. *Phosphorus, Sulfur Silicon Relat. Elem.* **1992**, *65* (1−4), 1−4.
(10) Bertermann, R.; Müller-Warmuth, W.; Jansen, C.; Hiltmann, F.; Krebs, B. NMR Studies of the Lithium Dynamics in Two Thioborate Superionic Conductors: $Li_9B_{19}S_{33}$ and $Li_{4-2x}Sr_{2+x}B_{10}S_{19}$ ($X \approx 0.27$). *Solid State Ionics* **1999**, *117* (3−4), 245−255.
(11) Conrad, O.; Jansen, C.; Krebs, B. Boron-Sulfur and Boron-Selenium Compounds—From Unique Molecular Structural Principles to Novel Polymeric Materials. *Angew. Chem., Int. Ed.* **1998**, *37* (23), 3208−3218.
(12) Sun, Z. D.; Chi, Y.; Xue, H. G.; Guo, S. P. A Series of Pentanary Inorganic Supramolecular Sulfides $(A_3X)[MB_{12}(MS_4)_3]$ (A = K, Cs; X = Cl, Br, I; M = Ga, In, Gd) Featuring $B_{12}S_{12}$ Clusters. *Inorg. Chem. Front.* **2017**, *4* (11), 1841−1847.
(13) Guo, S. P.; Chi, Y.; Liu, B. W.; Guo, G. C. Synthesis, Crystal Structure and Second-Order Nonlinear Optical Property of a Novel Pentanary Selenide $(K_3I)[InB_{12}(InSe_4)_3]$. *Dalt. Trans.* **2016**, *45* (25), 10459−10465.
(14) Sugimori, M.; Fukuoka, H.; Imoto, H.; Saito, T. Preparation and Crystal Structure of Chromium Silicon Selenide Containing a B_{12} Icosahedron with a Tunnel Structure. *J. Organomet. Chem.* **2000**, *611* (1−2), 547−550.
(15) Zheng, N.; Bu, X.; Feng, P. Synthetic Design of Crystalline Inorganic Chalcogenides Exhibiting Fast-Ion Conductivity. *Nature* **2003**, *426* (6965), 428−432.
(16) Bowes, C. L.; Ozin, G. A. Self-Assembling Frameworks: Beyond Microporous Oxides. *Adv. Mater.* **1996**, *8* (1), 13−28.
(17) Bag, S.; Trikalitis, P. N.; Chupas, P. J.; Armatas, G. S.; Kanatzidis, M. G. Porous Semiconducting Gels and Aerogels from Chalcogenide Clusters. *Science* **2007**, *317* (5837), 490−493.
(18) Trikalitis, P. N.; Rangan, K. K.; Bakas, T.; Kanatzidis, M. G. Varied Pore Organization in Mesostructured Semiconductors Based on the $[SnSe_4]^{4-}$ Anion. *Nature* **2001**, *410* (6829), 671−675.
(19) Foster, M. D.; Simperler, A.; Bell, R. G.; Friedrichs, O. D.; Paz, F. A. A.; Klinowski, J. Chemically Feasible Hypothetical Crystalline Networks. *Nat. Mater.* **2004**, *3* (4), 234−238.
(20) Wiedemeier, H.; von Schnering, H. G. Refinement of the Structures of GeS, GeSe, SnS and SnSe. *Z. Kristallogr. NCS.* **1978**, *148* (3−4), 295−303.
(21) Yao, H. G.; Zhang, R. C.; Ji, S. H.; Ji, M.; An, Y. L.; Ning, G. L. Mineralizer Effect on the Synthesis of Two Types of One-Dimensional Chains Silver-Selenogermanate and Selenostannate. *Inorg. Chem. Commun.* **2010**, *13* (11), 1296−1298.
(22) Nomura, T.; Maeda, T.; Takei, K.; Morihama, M.; Wada, T. Crystal Structures and Band-Gap Energies of $Cu_2Sn(S,Se)_3$ ($0 \leq x \leq 1.0$) Solid Solution. *Phys. Status Solidi Curr. Top. Solid State Phys.* **2013**, *10* (7−8), 1093−1097.
(23) Evain, M.; Queignec, M.; Brec, R.; Rouxel, J. $Ta_4P_4S_{29}$: A New Tunnel Structure with Inserted Polymeric Sulfur. *J. Solid State Chem.* **1985**, *56* (2), 148−157.
(24) Evain, M.; Queignec, M.; Brec, R.; Sourisseau, C. Chalcogen Substitution in the $Ta_4P_4S_{29}$ Tunnel Structure: Synthesis and Structure of $TaPS_6Se$. *J. Solid State Chem.* **1988**, *75* (2), 413−431.
(25) Mondloch, J. E.; Karagiaridi, O.; Farha, O. K.; Hupp, J. T. Activation of Metal-Organic Framework Materials. *CrystEngComm* **2013**, *15* (45), 9258−9264.

https://dx.doi.org/10.1021/acs.chemmater.0c04503
Chem. Mater. 2021, 33, 1723−1730